Journal of Materials Chemistry

Dynamic Article Links

Cite this: *J. Mater. Chem.*, 2011, **21**, 9350

www.rsc.org/materials

PAPER

MoO_3 nanoparticles dispersed uniformly in carbon matrix: a high capacity composite anode for Li-ion batteries

Tao Tao,[ab] Alexey M. Glushenkov,*[a] Chaofeng Zhang,[c] Hongzhou Zhang,[d] Dan Zhou,[d] Zaiping Guo,[c] Hua Kun Liu,[c] Qiyuan Chen,[b] Huiping Hu[b] and Ying Chen[a]

Received 15th January 2011, Accepted 26th April 2011
DOI: 10.1039/c1jm10220f

A MoO_3–carbon nanocomposite was synthesized from a mixture of MoO_3 and graphite by a controlled ball milling procedure. The as-prepared product consists of nanosized MoO_3 particles (2–180 nm) homogeneously distributed in carbon matrix. The nanocomposite acts as a high capacity anode material for lithium-ion batteries and exhibits good cyclic behavior. Its initial capacity exceeds the theoretical capacity of 745 mA h g^{-1} in a mixture of MoO_3 and graphite (1 : 1 by weight), and the stable capacity of 700 mA h g^{-1} (94% of the theoretical capacity) is still retained after 120 cycles. The electrode performance is linked with the unique nanoarchitecture of the composite and is compared with the performance of MoO_3-based anode materials reported in the literature previously (nanoparticles, ball milled powders, and carbon-coated nanobelts). The high value of capacity and good cyclic stability of MoO_3–carbon nanocomposite are attractive in respect to those of the reported MoO_3 electrodes.

1. Introduction

Rechargeable lithium-ion batteries (LIBs) have critical advantages in comparison with other types of rechargeable batteries because of their light weight and high energy density.[1] They are not only becoming the primary type of power sources for portable electronic devices (including cell phones, laptops and popular gadgets such as iPods) but also finding application in transportation, load leveling and storage of energy from renewable sources.[2] The total market for LiBs is currently estimated as 10 billion dollars per annum and continues to grow.[3] One of the biggest challenges in the LIB research is the development of practical electrode materials with high and stable capacities exceeding those of currently used electrode materials.

Molybdenum trioxide (MoO_3) is an attractive example of a prospective electrode material for LIBs with high capacity and has been evaluated as both cathode[4,5] and anode[6,7] materials. Application of MoO_3 as an anode material is particularly interesting. When tested in the potential window of 0.01–3.0 V *versus* lithium electrode, MoO_3 has been found to participate in a conversion reaction $MoO_3 + 6Li^+ + 6e^- \rightarrow 3Li_2O + Mo$. This proposed mechanism implies a high theoretical capacity of 1117 mA h g^{-1}, approximately three times larger than the theoretical capacity of a graphitic anode.[8,9] In practice, MoO_3 has poor ionic and electronic conductivity, and it fails to reach its theoretical capacity even if used in a nanostructured form. To the best of our knowledge, there is no report of achieving stable theoretical capacity in any nanostructured MoO_3 anode. A short summary of available results is provided in the following paragraph.

The electrochemical reactivity of ball-milled MoO_3 powders as an anode material has been investigated by Jung *et al.* and compared with that of bulk (unmilled) MoO_3 powders.[10] While bulk MoO_3 powder had a lower capacity and poorer cyclic performance (308 mA h g^{-1} in the tenth cycle), the ball milled oxide showed relatively enhanced performance (719 mA h g^{-1} in the 35th cycle) due to the reduction of particle size. In another study MoO_3 nanoparticles (with particle sizes of about 5–20 nm) showed a stable capacity of 630 mA h g^{-1} at the current rate of 0.5 C.[11] Bigger progress in improving experimental capacities of MoO_3 has been achieved recently. Hassan *et al.*[12] have coated MoO_3 nanobelts with carbon, and the carbon-coated nanobelts demonstrated a high capacity of about 1000 mA h g^{-1} at a current rate of 0.1 C. The capacity was increasing further upon cycling, which is, however, likely to be caused by a different effect, the formation of a polymeric layer, which is observed in many electrode materials operating *via* conversion reactions.[13] Electrode design appears to be a critical issue for achieving a high capacity according to Riley *et al.*[8] who managed to optimize the electrodes based on MoO_3 nanoparticles by melting binder-rich

[a]*Institute for Technology Research and Innovation, Deakin University, Waurn Ponds, VIC, 3217, Australia. E-mail: alexey.glushenkov@deakin.edu.au; Fax: +61 3 52271103; Tel: +61 3 52272931*
[b]*College of Chemistry and Chemical Engineering, Central South University, Changsha, 410083, China*
[c]*Institute for Superconducting and Electronic Materials, AIIM Facility, Innovation Campus, University of Wollongong, Squires Way, Fairy Meadow, NSW, 2519, Australia*
[d]*School of Physics, Centre for Research on Adaptive Nanostructures and Nanodevices (CRANN), Trinity College Dublin, Dublin 2, Republic of Ireland*

electrodes and redistributing a conductive additive uniformly. An optimized electrode demonstrated a high reversible capacity of about 1050 mA h g^{-1} at a current rate of 0.1 C after 30 cycles.

In this paper we propose an alternative way of designing a high-performance MoO_3-containing anode for Li-ion batteries. By employing a simple procedure of ball milling under a distinct milling mode with predominant shear action, we were able to prepare MoO_3 in the form of nanoparticles and simultaneously disperse them homogeneously in the carbon host, which acts as an excellent electronic conductor and electrochemically active component of the electrode at the same time. This highly uniform nanocomposite of MoO_3 and carbon with a weight ratio of 1 : 1 exhibits a high specific capacity, which exceeds the theoretical capacity (equal to 745 mA h g^{-1}) in the first 15 cycles and retains 94% of theoretical capacity (700 mA h g^{-1}) after 120 cycles at 0.2 C rate (149 mA g^{-1}). The capacity was completely stable between the 40th and 120th cycles. In addition to the excellent electrochemical performance of the composite material, it is important to note that conductive carbon black is not needed for the assembly of the electrode. The MoO_3/carbon nanocomposite reported here can be a prototype for future designs of high performance electrodes containing inorganic phases with low electronic and ionic conductivities.

2. Experimental section

Preparation of nanocomposite

1 g of a mixture of commercial MoO_3 powder (Sigma Aldrich, 99.9% purity) and graphite (weight ratio of 1 : 1) was loaded inside a stainless steel milling container together with four hardened steel balls (diameter of 25.4 mm). The powder was ball milled in a vertical rotating ball mill (described in detail elsewhere[14]) with a rotation speed of 75 rpm for 100 h at room temperature under argon atmosphere of 100 kPa. A schematic representation of the milling device and the milling mode used is shown in Fig. 1. This type of mill is usually used in conjunction with an external magnet; however, the magnet was intentionally removed in our preparation procedure to ensure the rolling action of balls.

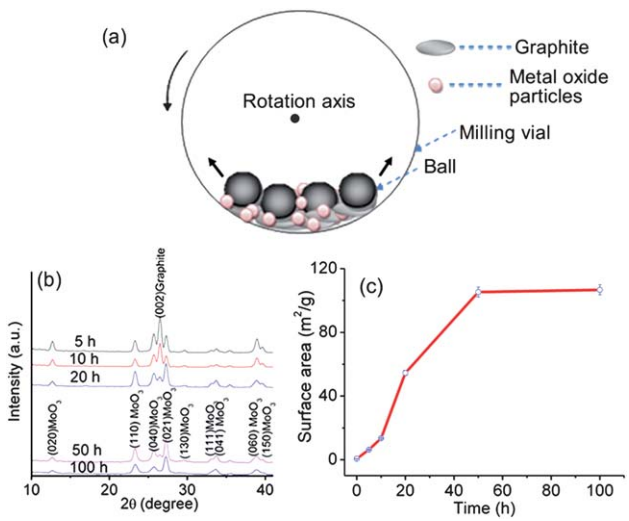

Fig. 1 Preparation of the MoO_3/C composite. (a) A schematic illustration of the milling procedure; (b and c) XRD patterns and surface areas of the ball milled mixture as functions of milling time (5–100 h).

Structural characterization

The samples were characterized by X-ray diffraction (XRD, PANalytical X-ray spectrometer, Cu X-ray source, $\lambda = 1.5418$ Å), scanning electron microscopy (SEM, Carl Zeiss UltraPlus operating under 20 kV) equipped with an energy-dispersive X-ray spectrometer (EDX, Oxford X-Max) and transmission electron microscopy (TEM, FEI Titan 80-300 operating under 300 kV). Surface areas of the samples were determined using a Micromeritics Tristar 3000 adsorption instrument.

Electrochemical measurement

The working electrodes were prepared by mixing 90 wt% of the as-prepared MoO_3/C materials with 10 wt% polyvinylidene difluoride (PVDF) binder in *N*-methyl-2-pyrrolidinone (NMP) to form homogeneous slurry, which was then uniformly pasted onto Cu foil. The working electrodes were dried in a vacuum oven at 100 °C for over 12 hours before assembling testing cells. Coin cells (CR2032 type) were assembled in an Ar-filled glove box (H_2O, $O_2 < 0.1$ ppm, Mbraun Unilab, USA). Li foil was used as the counter/reference electrode and a microporous polypropylene film was used as a separator. The electrolyte was 1 M $LiPF_6$ in a 1 : 1 (by volume) mixture of ethylene carbonate (EC) and dimethyl carbonate (DMC). The cells were galvanostatically discharged and charged over a voltage range of 0.01–3 V *vs.* Li/Li^+ at various current rates. A Land CT2001A cycler was used for electrochemical tests. All capacities and current rates were calculated per total mass of MoO_3 and carbon components.

3. Results and discussion

For those who are unfamiliar with the concept of ball milling, the general procedure of this method can be described as follows. A number of balls are loaded into a milling vial together with powders of interest, and the powders are modified by impact and sheer actions of the balls. The milling device used in this study can have distinct milling modes involving predominant sheer or impact action,[14] and the milling process adapted here is represented schematically in Fig. 1a. A cylindrical milling vial is rotated around a horizontal axis. The rotation of the vial causes rolling action of the balls at the bottom of the vial. Prior to operation, the mill is loaded with MoO_3 and graphite powders, and, being trapped between the surfaces of balls and the wall of the milling vial, these powders are getting processed by being subjected predominantly to sheer forces. The repeated mechanical action leads to a gradual decrease in the particle size and homogeneous mixing of the two powders at nanometre scale.[15]

XRD patterns of the MoO_3/C mixture are shown in Fig. 1b as a function of processing time. Only X-ray reflections of the starting orthorhombic MoO_3 (JCPDS no. 00-05-0508) and graphite are noticeable at all times, suggesting that no new crystalline phases are formed in the composite. The diffraction peaks of molybdenum oxide are getting visually less intense as milling time increases, and their typical widths increase,

indicating a gradual refinement of the average crystal size of MoO_3. Simultaneously, the 002 peak of graphite is becoming progressively smaller and disappears completely after 100 hours of milling. The structural changes in graphite can arise due to amorphisation or gradual slicing into nanometre-thin graphitic sheets.[16] The disappearance of the graphite's XRD pattern after 100 h coupled with broadening of the oxide peaks is an indication of significant structural changes in the composite. A dramatic degree of modification of the material's structure is also evident from the measurements of surface areas (Fig. 1c). The initially low surface area of 0.7 $m^2\ g^{-1}$ reaches a value of approximately 105 $m^2\ g^{-1}$ after 50 h of milling, and this value remains at a similar level after 100 h.

The microstructure of the composite obtained after 100 h of milling was further investigated using electron microscopy. The scanning electron microscope (SEM) image of the sample (Fig. 2a) shows that the composite consists of agglomerates with diameter about several hundreds of nanometres. Energy dispersive X-ray (EDX) elemental mapping has been used to evaluate the uniformity of distribution of molybdenum, oxygen and carbon elements. As shown in Fig. 2b–d, these three elements are distributed homogeneously in the product at the sub-micron scale. In addition to the three elements, the EDX spectrum (Fig. 2e) also indicates the presence of trace amounts of iron in the product introduced as a contamination from the milling media. A peak of silicon comes from the substrate used for holding the sample. It can be seen in Fig. 2b and c that the Mo and O elemental signals originate not only from the composite flake visible in Fig. 2a but also from the areas around it. These signals come from MoO_3 nanoparticles that detach from the composite during sample preparation (please refer to Fig. 4 and the related paragraph for more details).

The agglomerates observed in SEM were further investigated by a transmission electron microscope (TEM). Fig. 3a is a bright field image of a typical large agglomerate. Fig. 3b is the selected area diffraction pattern acquired from the agglomerate shown in

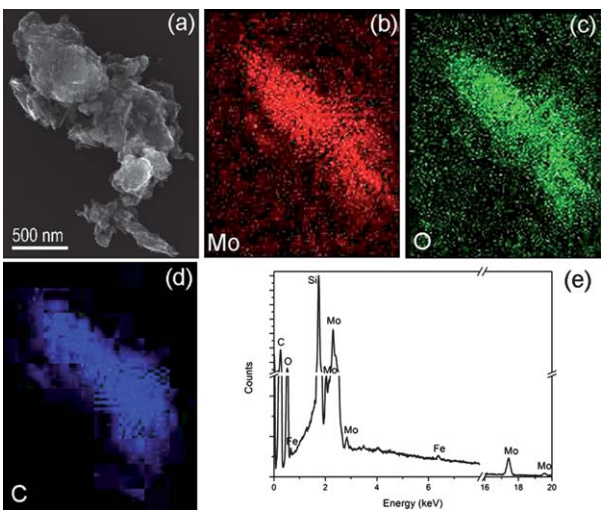

Fig. 2 SEM characterization of MoO_3/carbon nanocomposite. (a) Secondary electron image; (b–d) Elemental energy-dispersive X-ray (EDX) maps of molybdenum, oxygen and carbon, respectively; (e) EDX spectrum of the product.

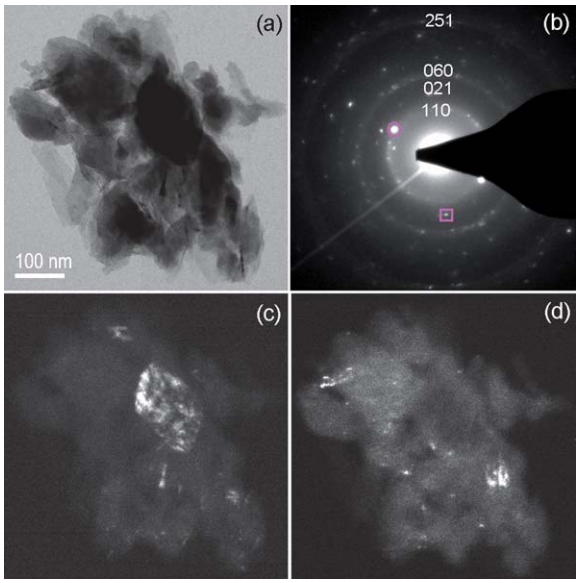

Fig. 3 TEM characterization of a typical large agglomerate. (a) Bright-field image; (b) electron diffraction pattern; (c and d) dark-field images taken using electron beams diffracted by {110} and {021} planes.

Fig. 3a. The diffusive diffraction rings and spots can be indexed using the structure of molybdenum trioxide (space group: *pbnm*) with lattice parameters $a = 3.92$ Å, $b = 13.94$ Å, and $c = 3.66$ Å. Dark field (DF) imaging enables direct correlation of the details of the image with the corresponding spots of the diffraction pattern. Two diffraction spots corresponding to {110} plane and

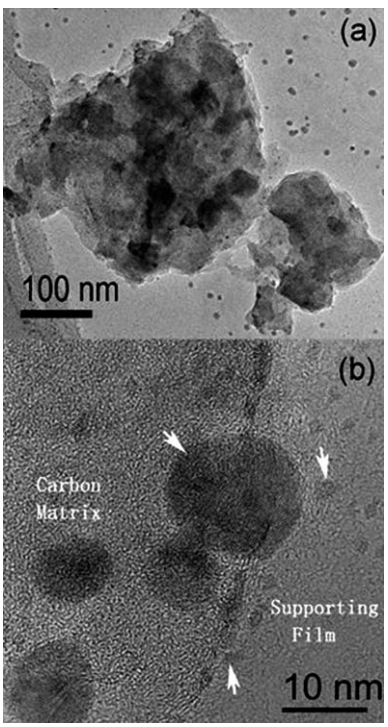

Fig. 4 Small nanoparticles of MoO_3 distributed in the matrix of carbon and on supporting film of the TEM grid. (a) Bright-field image; (b) high resolution image of a local area.

{021} plane (as indicated by the circle and open square in Fig. 3b) were used to form the DF images in Fig. 3c and d respectively. It reveals the granular structures of the large agglomerate shown in Fig. 3a and the sizes of the grains are up to 50–180 nm. It confirms that the composite contains aggregates of nanometre-sized particles distributed in carbon matrix.

MoO_3 nanoparticles with a typical diameter as small as 2–10 nm (black dots in Fig. 4a) were observed distributing sparsely but homogenously in large agglomerates. They can be found on the supporting carbon film as well, suggesting that the MoO_3 nanoparticles can be relocated from the composite onto the supporting film during the sample preparation. Fig. 4b shows a high-resolution TEM image of the nanoparticles and the carbon matrix of the composite. The lattice fringes of the nanoparticles (indicated by white arrows) correspond to the MoO_3 phase, which corroborates the EDX results. The carbon matrix hosting these nanoparticles is partially amorphous, but disordered lattice fringes can be easily spotted, for example, at the edge of the large particle in the aggregate.

Fig. 5a shows typical selected discharge/charge profiles of the MoO_3–C composite from the first 120 consequent discharge–charge cycles at a current density of 0.2 C in the voltage range of 0.01–3.0 V *vs.* Li/Li^+. The shape of the profiles did not change significantly during cycling, indicating an excellent capacity retention. The results indicate that the composite has high capacity and is electrochemically stable, which makes it a promising anode material for LIBs. Fig. 5b shows the cyclic behavior and Coulombic efficiency of the electrode. The first discharge capacity is 945 mA h g^{-1} and the first charge capacity is about 813 mA h g^{-1}. The initial capacity loss may result from the incomplete conversion reaction and irreversible lithium loss due to the formation of a solid electrolyte interphase (SEI) layer. The capacity gradually drops to the value of 700 mA h g^{-1} after the first 30 cycles and stays stationary at this level until the completion of the experiment. The Coulombic efficiency remains above 98% after the fifth cycle.

The rate capability of the nanocomposite is shown in Fig. 5c. The initial high capacity of ~806 mA h g^{-1} was observed at a current density of 0.2 C (149 mA g^{-1}) after three discharge/charge cycles. The capacity of the MoO_3/carbon composite was measured to be 650, 500, 365 and 240 mA h g^{-1} when the current rate was consecutively set at the levels of 0.5 C, 1 C, 2 C and 5 C. A capacity of ~780 mA h g^{-1} was detected in the 18th cycle when the current rate was returned to the value of 0.2 C.

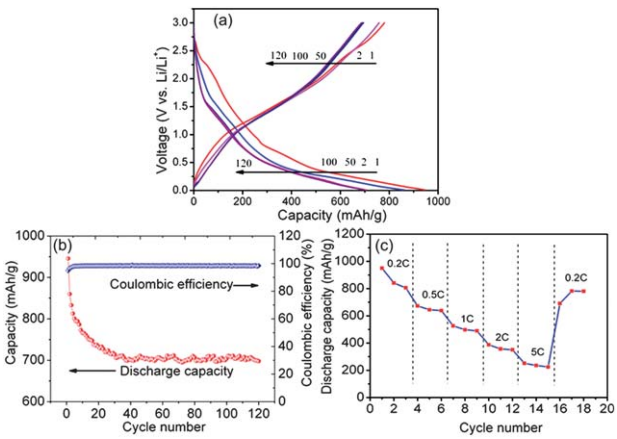

Fig. 5 (a) Selected discharge/charge profiles for the MoO_3/carbon (weight ratio of 1 : 1) composite at a current density of 149 mA g^{-1} (0.2 C); (b) discharge capacity and Coulombic efficiency of the composite for the first 120 cycles at 0.2 C; (c) rate capability of the composite.

The attractive electrochemical performance of the MoO_3/C nanocomposite is attributed to its unique structure, in which MoO_3 nanoparticles are uniformly dispersed in an electrically conductive carbon matrix. Such electrode design provides several significant advantages. Apart from increasing the conductivity of the electrode, the milled carbon component is electrochemically active itself and also provides mechanical framework preventing the electrode from disintegration during charge and discharge. Mechanical stability of the electrode is improved and the local loss of contact between electrode components is minimised. The high electronic conductivity of the carbon host compensates low conductivities of MoO_3 in the charged state and Li_2O in the discharged state because the electron transfer during the charge/discharge processes is greatly improved by the percolating carbon network. Small particles of MoO_3 reduce unwanted effects of slow Li diffusion in the oxide particles, efficiently accommodate volume changes during the reversible conversion reaction and provide reasonable rate capability. Similar enhanced electrochemical performance has been observed in other carbon-based nanocomposites including carbon nanotubes/SnO_2,[17] carbon/Si,[18] carbon/α-Fe_3O_4,[19] carbon nanofibers/CoO,[20] graphene/Mn_3O_4,[21] and graphene/Co_3O_4.[22] All of them exhibit large reversible capacities.

The discharge capacity of our MoO_3–carbon nanocomposite can be compared with capacities of MoO_3-based anodes reported in the literature previously,[8,10–12] and the relevant data are presented in Table 1. All capacities are calculated from the 30th cycle in the corresponding experiments. In order to compare the performance of the composite with that of MoO_3 materials correctly, we take into account that the theoretical capacity for MoO_3/carbon (1 : 1 by weight) composite (745 mA h g^{-1}) is different from that of molybdenum trioxide (1117 mA h g^{-1}). Therefore, the capacities expressed as percentages from corresponding theoretical capacities are compared.

As shown in Table 1, the electrode performance of the ball milled composite presented here is attractive in respect to that of previously reported MoO_3 electrodes. The capacity of a ball milled MoO_3 powder[10] was only 719 mA h g^{-1} (64.3% of the theoretical capacity) and it was measured at a very slow rate of 0.03 C. MoO_3 nanoparticles[11] have also demonstrated a low capacity 630 mA h g^{-1} (56.4% of the theoretical capacity), and these results are a reflection of poor ionic and electronic conductivity of MoO_3. It has been recently demonstrated that the electrodes based on MoO_3 nanoparticles can be fine tuned to achieve a high capacity of 1050 mA h g^{-1} (94% of the theoretical one). This result is close to the performance of our material (95.6% of the theoretical capacity in the 30th cycle) although we would like to highlight that it was demonstrated at a slower current rate (0.1 C *versus* 0.2 C in our experiments). In addition, the capacity in the optimized nanoparticle-based electrode was found to decrease gradually (900–950 mA h g^{-1} after 40 cycles) while, in contrast, 94% of theoretical capacity is retained by our electrode material after 120 cycles. Finally, it has been reported

Table 1 Discharge capacities of various reported MoO_3-based anodes for LIBs[a]

Material	C-Rate/C	Capacity/ mA h g^{-1}	Percentage of theoretical capacity	Reference
MoO_3–carbon (1 : 1) nanocomposite	0.2	712	95.6	This work
MoO_3 nanoparticles	0.5	630	56.4	11
Optimized electrodes with MoO_3 nanoparticles	0.1	1050	94	8
Ball-milled MoO_3	0.03	719	64.3	10
Carbon-coated MoO_3 nanobelts	0.1	1000	89.5	12

[a] All discharge capacities are calculated from the 30th cycle.

by Hassan *et al.* that the capacity of carbon-coated MoO_3 nanobelts can be above 1000 mA h g^{-1},[12] and 89% of theoretical capacity was measured in the 30th cycle. Based on the analysis of available literature data, a high capacity value and excellent cyclic stability of MoO_3–carbon nanocomposite are very attractive in respect to those of known MoO_3-based electrode materials.

The dependence of the discharge–charge performance on the composition of the MoO_3/C electrode is presented in Fig. 6, which shows the discharge capacity of several milled samples—pure graphite, MoO_3/graphite with weight ratios of 1 : 1, 7 : 3 and 9 : 1 as well as pure MoO_3 over the first 90 cycles. The tests were conducted at the current rates of 0.2 C calculated for each sample by taking into account their theoretical capacities. As it is evident from Fig. 6, milled MoO_3 and composites with different weight ratios show attractive capacities of 600–900 mA h g^{-1}. It is also interesting to note that the capacity of ball milled carbon (400 mA h g^{-1}) exceeds the theoretical capacity of graphite. A similar phenomenon of additional capacity has been observed previously in disordered carbons and several ways of explaining it have been suggested. Possible explanations include additional bulk storage, storage of lithium in cavities and nanopores, and surface/interfacial storage; these mechanisms are summarized in more detail in a recent review by Kaskhedikar and Maier.[23] The creation of nanoporous structure, necessary for some of these mechanisms, in graphitic carbons by ball milling has been previously demonstrated by Chen *et al.*[16]

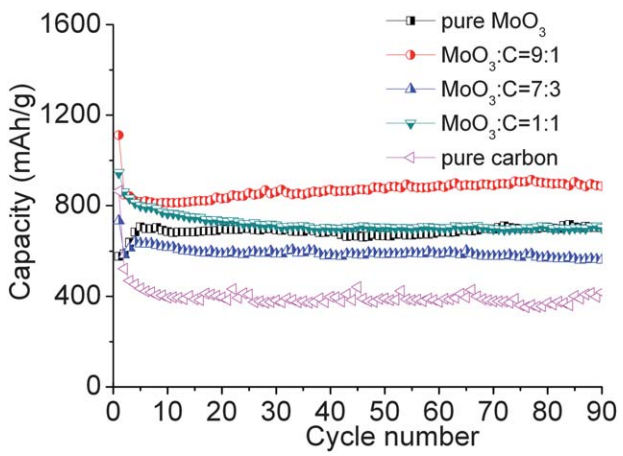

Fig. 6 Discharge capacities of various milled samples at the current rate of 0.2 C.

Table 2 Discharge capacities of MoO_3-containing electrodes with varied composition in the 50th cycle at a current rate of 0.2 C

Composition	Discharge capacity/ mA h g^{-1}	Percentage of the theoretical capacity (%)
Pure MoO_3	674	60
MoO_3 : C = 9 : 1	873	84
MoO_3 : C = 7 : 3	586	66
MoO_3 : C = 1 : 1	704	94

Discharge capacities of various MoO_3-containing samples calculated from the 50th cycle are shown in Table 2. Based on the result of this comparison, we may conclude that the weight ratio of 1 : 1 is the most practical since the capacity as high as 94% of the theoretical capacity can be retained after a large number of cycles.

4. Conclusion

We have demonstrated that the ball milling method can prepare a highly uniform nanocomposite of MoO_3 and carbon, which can perform as an advanced anode material for high capacity lithium-ion batteries. The MoO_3/C nanocomposite with a weight ratio of 1 : 1 exhibits a high reversible capacity as high as 700 mA h g^{-1} at 0.2 C rate (149 mA g^{-1}) after 120 cycles, which matches closely the theoretical capacity of 745 mA h g^{-1} for such a composite. This promising electrochemical performance is a result of the unique nanostructure of the composite. Small MoO_3 nanoparticles (with a size range of 2–180 nm) are uniformly dispersed in an electrically conductive carbon host, and such nanoarchitecture brings a number of advantages for the electrode performance and suppresses capacity degradation after multiple cycles.

Acknowledgements

Financial support from the Australian Research Council under the Centre of Excellence program is acknowledged. Mr Tao Tao thanks the National Basic Research Program of China (No: 2007CB613601) and the China Scholarship Council (CSC) for providing his scholarship. The work conducted in Trinity College Dublin is supported by the Irish Government's Programme for Research in Third Level Institutions, Cycle 4, National Development Plan 2007–2013 within the framework of the INSPIRE programme and Science Foundation Ireland under Grant 07/SK/I1220a.

Notes and references

1 M. Yoshio, R. J. Brodd and A. Kozawa, *Lithium-Ion Batteries. Science and Technologies*, Springer, New York, 2009.
2 P. G. Bruce, B. Scrosati and J. M. Tarascon, *Angew. Chem., Int. Ed.*, 2008, **47**, 2930.
3 C. M. Park, J. H. Kim, H. S. Kim and H. J. Sohn, *Chem. Soc. Rev.*, 2010, **39**, 3115.
4 W. Y. Li, F. Y. Cheng, Z. L. Tao and J. Chen, *J. Phys. Chem. B*, 2006, **110**, 119.
5 L. Q. Mai, B. Hu, W. Chen, Y. Y. Qi, C. S. Lao, R. S. Yang, Y. Dai and Z. L. Wang, *Adv. Mater.*, 2007, **19**, 3712.
6 N. A. Chernova, M. Roppolo, A. C. Dillon and M. S. Whittingham, *J. Mater. Chem.*, 2009, **19**, 2526.
7 J. S. Chen, Y. L. Cheah, S. Madhavi and X. W. Lou, *J. Phys. Chem. C*, 2010, **114**, 8675.
8 L. A. Riley, S. H. Lee, L. Gedvilias and A. C. Dillon, *J. Power Sources*, 2010, **195**, 588.
9 T. Tsumura and M. Inagaki, *Solid State Ionics*, 1997, **104**, 183.
10 Y. S. Jung, S. k. Lee, D. J. Ahn, A. C. Dillon and S. H. Lee, *J. Power Sources*, 2009, **188**, 286.
11 S. H. Lee, Y. H. Kim, R. Deshpande, P. A. Parilla, E. Whitney, D. T. Gillaspie, K. M. Jones, A. H. Mahan, S. B. Zhang and A. C. Dillon, *Adv. Mater.*, 2008, **20**, 3627.
12 M. F. Hassan, Z. P. Guo, Z. Chen and H. K. Liu, *J. Power Sources*, 2010, **195**, 2372.
13 J. Cabana, L. Monconduit, D. Larcher and M. R. Palacín, *Adv. Mater.*, 2010, **15**, E170.
14 A. Calka and A. P. Radlinski, *Mater. Sci. Eng., A*, 1991, **134**, 1350.
15 Y. Chen, T. Hwang, M. Marsh and J. S. Williams, *Metall. Mater. Trans. A*, 1997, **28**, 1115.
16 Y. Chen, J. F. Gerald, L. T. Chadderton and L. Chaffron, *Appl. Phys. Lett.*, 1999, **74**, 2782.
17 Y. B. Fu, R. B. Ma, Y. Shu, Z. Cao and X. H. Ma, *Mater. Lett.*, 2009, **63**, 1946.
18 A. Magasinski, P. Dixon, B. Hertzberg, A. Kvit, J. Ayala and G. Yushin, *Nat. Mater.*, 2010, **9**, 535.
19 S. L. Chou, J. Z. Wang, D. Wexler, K. Konstantinov, C. Zhong, H. K. Liu and S. X. Dou, *J. Mater. Chem.*, 2010, **20**, 2092.
20 W. L. Yao, J. Q. Chen and H. W. Cheng, *J. Solid State Electrochem.*, 2011, **15**, 183.
21 H. L. Wang, L. F. Cui, Y. Yang, H. S. Casalongue, J. T. Robinson, Y. Y. Liang, Y. Cui and H. J. Dai, *J. Am. Chem. Soc.*, 2010, **132**, 13978.
22 Z. S. Wu, W. C. Ren, L. Wen, L. B. Gao, J. P. Zhao, Z. P. Chen, G. M. Zhou, F. Li and H. M. Cheng, *ACS Nano*, 2010, **4**, 3187.
23 N. A. Kaskhedikar and J. Maier, *Adv. Mater.*, 2009, **21**, 2664.